Neuronal activity and AMPA-type glutamate receptor activation regulates the morphological development of oligodendrocyte precursor cells

Fannon, Jessica; Tamier, Wysnavie; Fulton, Daniel

DOI:
10.1002/glia.22799

Document Version
Peer reviewed version

Citation for published version (Harvard):
Fannon, J, Tamier, W & Fulton, D 2015, 'Neuronal activity and AMPA-type glutamate receptor activation regulates the morphological development of oligodendrocyte precursor cells', *GLIA*, vol. 63, no. 6, pp. 1021-1035. https://doi.org/10.1002/glia.22799

Neuronal activity and AMPA-type glutamate receptor activation regulates the morphological development of oligodendrocyte precursor cells

Jessica Fannon[1], Wysnavie Tarmier[2] and Daniel Fulton[1,2]

[1] School of Life Sciences, University of Warwick, Coventry, UK. [2] Neurotrauma Research Group, Neurobiology Section, School of Clinical and Experimental Medicine, College of Medical and Dental Sciences, University of Birmingham, Birmingham, UK.

Running title: AMPAR regulation of OPC morphology

Correspondence to: Daniel Fulton, Ph.D. Neurotrauma Research Group, Neurobiology Section, School of Clinical and Experimental Medicine, College of Medical and Dental Sciences, University of Birmingham, Edgbaston, Birmingham, B152TT. Email: d.fulton@bham.ac.uk. Tel:+44-1214-148441.

Number of figures: 7. Number of text pages: 38. Number of words in abstract: 249 words. Number of words in methods: 2301 words. Number of words in introduction: 576 words. Number of words in results: 1440 words. Number of words in discussion: 2366 words. Number of words in references: 1265 words. Number of words in legends: 1230 words. Number of words in acknowledgements: 127 words. Total words count: 9554 words.

Keywords: Oligodendrocyte precursor cell, NG2 glia, neuronal activity, AMPA receptor, NMDA receptor, process morphology, proliferation, differentiation, myelination

Main Points:

1. Blockade of neuronal activity and AMPA receptors reduces OPC process extension and branching in cerebellar slice cultures

2. Inhibiting neuronal activity and AMPA receptors increased OPC proliferation and differentiation, but reduced myelination
3. Blockade of NMDA receptors did not affect the proliferation, differentiation or morphological development of OPC

This is the accepted version of the following article: Fannon J, Tarmier W, Fulton D. 2015. Neuronal activity and AMPA-type glutamate receptor activation regulates the morphological development of oligodendrocyte precursor cells. Glia. 63:921-1099, which has been published in final form at: http://onlinelibrary.wiley.com/doi/10.1002/glia.22799/abstract

ABSTRACT

Myelination is initiated when oligodendrocyte precursor cells (OPC) contact target axons. Neuronal activity promotes myelination through actions that may involve OPC AMPA and NMDA glutamate receptors (AMPAR, NMDAR). Therefore, activity and AMPAR / NMDAR activation are predicted to promote the morphological development of OPC. AMPAR can regulate OPC development, but this analysis was not performed *in situ* and the role of action potentials was not examined. Hence, the influence of activity and AMPAR on OPC morphology and development remain untested in the CNS where axon-glial interactions are preserved. Data on NMDAR are mixed with conflicting results from *in vitro* and *in vivo* work. To gain a fuller understanding of activity-dependent OPC development *in situ*, we explored the role of AMPAR and NMDAR in cerebellar slice cultures that permit the study of endogenous OPC development and myelination. The structure of individual OPC was resolved from cells labelled with membrane targeted GFP. Morphological data were then validated against assays of OPC development. Blocking either activity or AMPAR impaired the morphological development of OPC and promoted proliferation and differentiation. Increasing the pool of oligodendrocytes (OL) by blocking activity or AMPAR failed to promote myelination. Instead both myelination and the expression of myelin basic protein were reduced by these treatments suggesting that full differentiation to a myelinating phenotype did not occur. Blocking NMDAR left OPC proliferation, differentiation and morphology unchanged. These data indicate an important role for AMPAR but not NMDAR in mediating the activity-dependent signals that regulate OPC morphology, development and myelination.

INTRODUCTION

Electrical activity within axons influences oligodendrocyte (OL) development and myelin formation (Demerens et al., 1996; Gibson et al., 2014; Stevens et al., 2002; Wake et al., 2011). Unfolding the relationships that connect axonal activity to myelination may provide valuable insights into myelin repair in the CNS. Glutamate released from axons is positioned to mediate these activity-dependent actions. precursor cells (OPC) express functional AMPA and NMDA type glutamate receptors (AMPAR, NMDAR) with the latter enabling these cells to sense axonal action potentials (for reviews see Bakiri et al., 2009; Gallo et al., 2008). Moreover, *in vitro* analyses of OPC isolated from the developing CNS and cultured brain slices reveals alterations in OPC development following modulation of these receptors. Blockade of AMPAR increases OPC proliferation and the number of cells expressing later stage markers for OPC (04 antigen) and OL (01 antigen) (Yuan et al., 1998), and in the context of NMDAR function, stimulation of NMDAR increases the expression of myelin basic protein (MBP) (Li et al., 2013), while blockade of these receptors disrupts activity-dependent increases in MBP expression associated with electrical stimulation (Wake et al., 2011). To date, studies examining activity and neurotransmitter-dependent development have largely focussed on the analysis of proliferation, and the expression of developmental marker proteins. Consequently, less is known about other features of OPC biology that are affected by axonal activity and glutamate signalling.

The migration of OPC and their connection to target axons, key behaviours underlying myelination, demand marked alterations in OPC process morphology. Data from primary cultures indicate that neuronal activity and NMDAR activation influence the morphology of OPC (Stevens et al., 2002; Li et al., 2013) and, in line with these findings, NMDAR activation also promotes their migration (Xiao et al., 2013). To our knowledge

the impact of AMPAR function on OPC morphology has not been addressed. However, AMPAR stimulation increases the migration of isolated OPC (Gudz et al., 2006). Together these data on AMPAR and NMDAR suggest that these receptors regulate OPC process dynamics. The relevance of these *in vitro* data to OPC development *in vivo* requires further validation for two reasons. First, the morphology of OPC and OL in primary culture differs from that seen in CNS tissue. Second, findings from isolated OPC may not agree with those obtained in the intact CNS. For example, mice bearing a deletion of the NR1 subunit during embryonic and postnatal development display normal OPC development and myelination (De Biase et al., 2011), while modulation of NMDAR *in vitro* affects OPC differentiation and morphological development (Li et al., 2013). Thus, if activity-dependent signals are to be exploited in the context of myelin repair, it is first necessary to clarify how axonal activity and AMPAR/NMDAR activation influence the morphological development of OPC within more intact CNS environments. To this end, we analysed the influence of neuronal activity and AMPAR / NMDAR function on the structural development of OPC in cerebellar slices, cultured under conditions designed to modulate neuronal activity and activity-dependent signalling pathways during myelination (Birgbauer et al., 2004). Detailed morphological reconstructions were then obtained from OPC transduced by recombinant virus carrying membrane tethered GFP. Findings from this approach were validated and extended by established assays of OL development (proliferation, lineage progression) and myelination. These studies provide new data on the structural response of OPC to neuronal activity, indicate a role for AMPAR, but not NMDAR, in these actions, and provide new findings on the role of neuronal activity and AMPAR in myelination.

MATERIALS AND METHODS

Animals

All Experiments were performed on organotypic cerebellar slice cultures obtained from 50% C57BL/6J 50% CBA/CaCrl mice (male and female). In total 29 animals (male and female, ranging from post-natal day 8-11 in age) were used for these experiments. All mice were bred in house at the University of Warwick and were killed according to humane methods proscribed in Schedule 1 of the Animals (Scientific Procedures) Act 1986.

Experimental design

Except where indicated, experiments followed the same design (Fig 1A). Slice cultures were maintained *in vitro* for 6 days prior to commencement of drug incubation. Drugs were applied for 48 hours with replacement after 24 hours. In some experiments BrdU (5-Bromo-2'-deoxyuridine, Sigma-Aldrich Company Ltd, Dorset, UK) was included in this drug replacement medium. Viral infections (see below) were also carried out at this time-point in experiments examining OPC morphology. Drug and BrdU treatments were terminated after 48 hours by replacement with control culture medium, after which slice cultures were fixed and processed for immnunohistochemical analysis and imaging.

Organotypic slice cultures

Slice cultures were prepared according to the methods described by De Simoni and Yu (2006) with the following modifications. Six-well culture plates were prepared at least 1 hour before plating. Culture inserts (Merk Millipore, MA, USA) were placed into wells containing 1 mL of culture medium before equilibration in a humidified cell culture incubator (37°C, 5% CO_2). Culture medium consisted of 50% MEM with glutamax, 25%

EBSS, 25% horse serum, glucose (0.13 mg/mL) and penicillin / streptomycin. For experiments involving viral transduction, small pieces of confetti membrane (Merk Millipore) placed on top of the culture inserts provided a substrate for the removal and transfer of individual slices. Pups were killed by cervical dislocation and brains rapidly removed and placed in oxygenated ice-cold slice preparation solution for 5 minutes. Slicing solution contained the following compounds (in mM): 25.95 $NaHCO_3$, 1.39 NaH_2PO_4, 10 glucose, 124 NaCl, 2.95 KCl, 100 $MgCl_2$, 2 $CaCl_2$, 5000 units/mL penicillin/streptomycin. Brains were then transferred to petri dishes containing ice-cold slice solution after which the cerebellum was isolated and the lateral lobes removed to provide a parasaggital surface for gluing to the vibratome chuck. Parasagittal slices (350 μm) were cut by vibratome (Zeiss HM 650V, Zeiss, Oberkochen, Germany) in oxygenated ice-cold slice solution, and then transferred in the tip of a cut-down P1000 pipette to the membrane of the culture insert. Typically 4 to 7 slices were plated on each insert. Slices were maintained in a humidified incubator (37°C, 5% CO_2) for 7 to 10 days with medium changes every 2 to 3 days.

Semliki Forest Virus preparation

Recombinant Semliki Forest Virus subtype A7(74) (SFVA7(74) transduces OL lineage cells and astrocytes in organotypic brain slices (Ehrengruber et al. 2003; Haber et al., 2006; 2009). In the present work SFVA7(74) delivered farnesylated eGFP (GFPf) to a proportion of OPC in cerebellar slice cultures allowing imaging and detailed resolution of individual OPC (e.g. Fig. 3Bi-ii). Plasmids for SFVA7(74)-GFPf and Helper2 were kindly provided by Markus Ehrengruber (Kantonsschule Hohe Promenade, Zurich). Infectious SFVA7(74)-GFPf (SFV-GFPf) particles were generated in BHK cells using the methods described by Ehrengruber et al. (2011). The un-purified viral preparation was then aliquoted and stored at -80 °C.

Viral infection of slice cultures

For infection of OPC, 10 µL of undiluted viral stock (6.5 x 10^6 infectious units / mL) was dispensed directly onto the top of slices. Slices were then returned to the incubator and cultured for a further 15 to 24 hours when strong GFPf expression could be detected under epifluorescent illumination.

Drugs

Stock solutions of TTX (voltage-operated Na^+ channel inhibitor) (1 mM, Ascent Scientific, Cambridge, UK,), GYKI (AMPAR inhibitor) (9.74 mM), D-AP5 (100 mM) and MK-801 (10 mM) (NMDAR inhibitors) were prepared in distilled water. GYKI, D-AP5 and MK-801 were purchased from Tocris Bioscience (Abingdon, UK). For application to slice cultures, drugs were diluted in culture medium. Final concentrations were: TTX 1 µM; D-AP5 50 µM (all AP5 experiments save Figure 6D); MK-801 10 µM (all MK-801 experiments save Figure 6D); GYKI 25 µM. This concentration of GYKI is slightly above the $_{IC}50$ value for AMPAR (~9.8 µM, Paternain et. al., 1995), but well below that for Kainate receptors (450 µM, Paternain et. al., 1995), which are also expressed by OPC (Patneau et al., 1994). GYKI is not reported to inhibit NMDAR (Ouardouz and Durand, 1991), therefore this concentration of GYKI is likely to have achieved an effective blockade of AMPAR, while avoiding off-target effects on other glutamate receptors. BrdU stock solution was prepared in sterile PBS (32.5 mM) and used at a final concentration of 10 µM.

Immunohistochemistry

Prior to processing for immunohistochemistry slices grown directly on culture inserts were cut from the insert with a scalpel. Cutting was performed in the lid of a 100 mm petri dish part filled with PBS. After freeing from the insert, slices were carefully transferred to a square of parafilm mounted in a 100 mm petri dish. Slice cultures

grown on confetti membranes were transferred directly to the parafilm without the need for cutting. Mounting on parafilm allowed subsequent immunohistochemistry in small volumes (60-100 µL). Once placed on the parafilm, slice cultures were fixed overnight at 4°C with 4% paraformaldehyde (PFA), washed 4 times in phosphate buffered solution (PBS) and incubated in blocking solution (PBS with 10% normal goat serum (NGS) and 0.2% Triton-X100) for 4-5 h at room temperature under constant agitation. Slices were then incubated overnight (minimum of 15 h) in primary antibodies diluted in carrier solution (PBS with 10% NGS and 0.05% Triton-X100). Following primary incubations, slices were rinsed 4 times in PBS before incubation with the appropriate secondary antibodies (4-6 h, room temperature under agitation). Slice cultures were then rinsed 4 times and blotted gently before mounting on microscope slides. Finally, a drop of aqueous mounting medium (Aquamount, Lerner Laboratories, Pittsburgh, PA, USA) was added to each slice before coverslipping.

Antibodies

In experiments examining OPC morphology, SFV-GFPf infected OPC were identified with rabbit polyconal anti-NG2 (1:200, Merk Millipore). Proliferation of OPC was examined by dual labelling with rabbit polyclonal anti-olig2 (1:500, Merk Millipore), a marker present at all stages of OL development, and rat polyclonal anti-BrdU (1:200, Abcam, Cambridge, UK). Differentiation of OPC was determined by dual staining with rabbit polyconal anti-olig2 (as above) and mouse anti-adenomatus polyposis coli / CC1 (1:500, EMD chemicals, Gibbstown, NJ, USA). Myelination was examined by dual labelling with rat-anti MBP (1:200, Merk Millipore) and chicken anti-NF200 (1:10,000, Abcam). Primary antibodies were detected with Alexa Fluor® (AF) conjugated Goat IgG antibodies (Invitrogen, San Diego, CA, USA) raised against the appropriate species, except for CC1 which was labelled with AF conjugated donkey IgG antibody. For proliferation studies, anti-olig2 was detected with AF-594 and anti-BrdU with AF-488.

In the differentiation experiments, anti-olig2 was detected with AF-488 and anti-CC1 with AF-594 and, for myelination studies, anti-MBP detected with AF-488 and anti-NF200 with AF-594. For dual immunofluorescent labelling, the specificity of primary-secondary antibody immunoreactions was confirmed by incubation of slice cultures with one primary antibody omitted, subsequently followed by incubation with both secondary antibodies. This procedure was performed for each primary antibody, and for all combinations of antibodies used in the study. In all cases we were able to confirm specificity.

Confocal Imaging and image analysis

Individuals blinded to the experimental conditions conducted the imaging and analyses. Unless otherwise stated images were acquired from cerebellar white matter, molecular, purkinje cell, and granule cell layers, with data from the different regions being analysed together.

OPC Proliferation and Differentiation

Experiments with TTX and GYKI. Fluorescent images (512 by 512 pixels, 2 line average) were captured using a Leica TCS SP2 confocal microscope (Leica Microsystems) operating in sequential scan mode. 3 μm Z stacks (0.5 μm steps for proliferation, 1 μM steps for differentiation) were collected with a 40x 1.25 N.A. oil immersion objective (HCX Plan APO; Leica Microsystems) and processed using NIH ImageJ (Schneider et al., 2012). Image stacks were converted to maximum intensity projections (MIP), thresholded, and colocalised pixels identified with the Colocalisation Highlighter ImageJ plugin (see Fig 1Biii for example of a colocalisation image). The total number of olig2$^+$ and olig2$^+$/BrdU$^+$ cells (proliferation), or olig2$^+$ and olig2$^+$/CC1$^+$ cells (differentiation), were counted using the ITCN nuclei counting ImageJ plugin (Thomas Kuo and Jiyun Byun, Center for Bio-image Informatics, UC Santa Barbara) and the proportion of the

total olig2^{+} population expressing either BrdU or CC1 determined. For the proliferation experiment quantitative data were determined from a total of 100 control images, 50 GYKI images and 100 TTX images. For the differentiation experiment data were averaged from a total of 196 control images, 229 GYKI images and 203 TTX images. Prior to these analyses we successfully validated the use of the colocalisation highlighter and ITCN plugins on slice culture-derived images by cross-checking plugin derived colocalisation images with single-channel merged images, and by comparing ITCN cell counts with those obtained by manual means.

Experiments with AP5 and MK-801. Drugs were applied for 48 hours starting from 7 DIV. Fluorescent images stacks (630 by 1005 pixels, 3 µm volume, 1 µm steps) were acquired using a differential spinning disk confocal microscope (Revolution DSD, Andor Technology plc, Belfast, UK) equipped with a 20x Air Objective (0.5 N.A.). Images were processed and colocalisation assessed as described above. For the proliferation experiment quantitative data were determined from a total of 205 control images, 203 AP5 images and 302 MK-801 images. For the differentiation experiment data were averaged from a total of 184 control images, 195 AP5 images and 172 MK-801 images. Data displayed in 6B were averaged from174 control images, 170 AP5 images and 170 MK-801 images.

Differences in mean control levels of proliferation and differentiation between studies are explained by differences in age of tissue used for slice preparation, which ranged from P8 to P11, since all other conditions, e.g. methods for slice preparation and culture conditions, were kept the same.

Myelination.

Myelination was assessed by examining colocalisation of myelin (MBP) and axonal (NF200) immunoreactivity (Birgbauer et al., 2004) in the granule cell layers adjacent to cerebellar white matter. Slice cultures were treated with TTX or GYKI for 48-hours starting at 3 DIV, after which they were maintained in normal culture medium for a further 7 days to provide sufficient time for potential impacts on myelination to develop. Slices were then fixed and immunostained for anti-NF200 and anti-MBP (Fig. 4A-C). Fluorescent images stacks (5 μm volume, 1 μm steps) were captured using the imaging system described for AP5 and MK801 experiments, and then processed for colocalisation analysis as previously described. Quantitative data were determined from a total of 88 control images, 87 GYKI images and 49 TTX images.

Morphological analysis of OPC with SFV-GFPf.

$GFPf^+$ OPC were identified by their distinct morphology under epifluorescent illumination. OPC had small irregular shaped cell bodies with a faint cytoplasmic GFP signal and a crisp GFP^+ border indicative of GFPf targeting to the plasma membrane (Fig. 3Ai). OPC also displayed complex finely branching GFP^+ process fields (Fig. 3Bii, Cii, Dii). The OPC status of each cell was validated by confirmation of NG2 immunofluorescence (Fig. 3Ai-iii). For experiments using TTX and GYKI confocal image stacks (500 by 1024 pixels, 2 line average, 0.5 μm steps) of $GFPf^+$ $NG2^+$ OPC were collected with a 40x 1.25 N.A. oil objective. Photomultiplier gain and stack volume were adjusted to capture the complete cell and achieve the greatest definition of faintly labelled processes. Detailed morphological reconstructions were prepared using NeuronStudio software (Computational Neurobiology and Imaging Center, Icahn School of Medicine at Mount Sinai; Wearne et al. 2005). Cells were traced manually from MIP images and ambiguous process paths were resolved by viewing images in three-dimensions using the stack viewer mode. NeuronStudio's Sholl analysis function was then used to derive

quantitative process field data from these reconstructions. Data were determined from a total of 27 reconstructions for each treatment.

While NeuronStudio provided accurate models of OPC process fields, the manual tracing method proved costly in terms of time. WIS-NeuroMath (NeuroMath), a recently published non-commercial automated tracing software (Weizmann Institute of Science, Rehovot, Israel; Rishal et al., 2013) provided a more time-efficient method for tracing OPC. This manual tracing method was used in experiments investigating the effects of D-AP5 and MK-801 on OPC morphology (Fig. 7). Fluorescent image stacks (1024 by 1024 pixels, 2 line average, 0.5 μm) were collected on a Zeiss 510 confocal microscope using a 40x water immersion objective. 2D reconstructions were then generated in NeuroMath (Fig. 7A,B), and quantified for total process length and total branch points using NeuroMath's cell measurement output. Reconstructions were subjected to further analysis using the ImageJ Sholl Analysis plugin (Sholl Analysis v1.0) to yield measurements of maximum process extension, and to provide information on the spatial distribution of process fields.

We validated the NeuroMath automated tracing method by comparing it directly with data analysed manually using NeuronStudio (Supplementary Results, Fig. S1, S2). Overall, the results of these comparisons indicate that the automatic tracing method provides a reliable means to make within experiment comparisons, and that the use of two different tracing approaches is justified so long as conclusions are only drawn from within methods comparisons.

Data analysis and statistics

Normal distributions in each data set were tested using Kolmogorov-Smirnov tests. For data with normal distributions, single between-group comparisons were made by t-

tests, and multiple comparisons were investigated by one-way ANOVA followed by Tukey's multiple comparison tests to detect pair-wise between-group differences. When normal distributions were absent, nonparametric Mann-Whitney U tests and Kruskal-Wallis tests were used respectively for two-group and multiple group comparisons, with between-group differences checked by Dunn's multiple comparisons test. All statistical tests were computed with Prism 3.0 (Graphpad Software, Inc., El Camino Real, CA, USA). A fixed value of $P_{\alpha}<0.05$ for two-tailed tests was the criterion for reliable differences between groups. Cited values were $\overline{X}$s $\pm$ SEMs, unless otherwise noted.

RESULTS

Neuronal activity and AMPAR activation regulate OPC proliferation

Previous studies using cells dissociated from slice cultures showed that blockade of AMPAR increased OPC proliferation (Yuan et al., 1998). To validate these results *in situ* and explore a potential contribution of neuronal activity to this effect we examined the effect of TTX and GYKI on OPC proliferation. Confocal analysis of olig2 and BrdU signals within intact slice cultures revealed a significant increase in the fraction of $BrdU^+$ $Olig2^+$ cells in slices treated with either TTX (Fig. 1C, 1E) or GYKI (Fig. 1D, 1E) (ANOVA, $F(2,249)= 5.73$, $P < 0.01$, control vs TTX $P < 0.01$, control vs GYKI $P < 0.05$). These data confirm that blockade of either neuronal activity or AMPAR function enhances proliferation of OPC within intact cerebellar slice cultures.

Neuronal activity and AMPAR activation regulate OPC differentiation

To determine whether increases in the OPC population generated by TTX and GYKI are accompanied by an increase in the differentiation of these cells we quantified the ratio of mature OL to total OL lineage cells. Blockade of either neuronal activity (Fig. 2B, 2D) or AMPAR (Fig. 2C, 2D) significantly increased the proportion of OL lineage cells

displaying CC1 signal (KW = 121, df = 2, $P < 0.001$, control vs TTX $P < 0.001$, control vs GYKI $P < 0.001$). This result indicates that blockade of neuronal activity or AMPAR promotes differentiation leading to an increase in the generation of OL.

Neuronal activity and AMPA type glutamate receptors regulate OPC morphology

SFV-GFPf has previously been used to label OPC in slice cultures (Haber et al., 2009). Using this method Haber et al. (2009) were able to resolve OPC processes and detect slow changes in process morphology. Therefore we chose to use this method to examine the developmental actions of neuronal activity and AMPAR on OPC morphology. Slices were treated with TTX and GYKI and SFV-GFPf infected OPC identified by expression of NG2 (Fig. 3Ai-iii). OPC treated with either TTX (Fig. 3Ci-iii) or GYKI (Fig. 3Di-iii) displayed marked changes in the morphology of their processes. Both TTX and GYKI induced a significant reduction in total process length (Fig. 3E) (ANOVA, $F(2,78)= 5.76$, $P < 0.01$, control vs TTX $P < 0.05$, control vs GYKI $P < 0.05$) and process branch points (Fig. 3F) (ANOVA, $F(2,78)= 4.49$, $P < 0.05$, control vs TTX $P < 0.05$, control vs GYKI $P < 0.05$). Together these data suggest that both neuronal activity and AMPAR activation promote the elongation and branching of OPC processes.

Expansion of the oligodendrocyte population after activity and AMPAR blockade does not enhance myelin formation

The temporary blockade (48 hours) of neuronal activity or AMPAR produced an increase in the proliferation and differentiation of OPC and altered their structural properties (Fig. 1, 2, 3). The additional $CC1^+$ OL generated under these conditions could increase the pool of OL capable of myelinating cerebellar axons, leading to enhanced myelination. To test this possibility we examined myelination 7 days after exposing slice cultures to either TTX (Fig. 4B) or GYKI (Fig. 4C). The colocalisation index for MBP/NF200 was significantly reduced in slice cultures treated with either TTX or GYKI

(ANOVA, F(2,221)= 33.51, $P < 0.001$, control vs TTX $P < 0.001$, control vs GYKI $P < 0.001$) (Fig. 4D). These data suggest that the additional $CC1^+$ OL induced by blockade of neuronal activity or AMPAR do not contribute to the myelination of cerebellar axons. While visual inspection did not reveal obvious differences between the level of MBP immunoreactivity (Fig. 4, c.f. Aii, Bii, Cii), comparison of the average MBP signal detected from control, TTX and GYKI treated slice cultures revealed a significant reduction in the expression of MBP after TTX and GYKI treatment (Fig. 4E)(KW = 61.06, df = 2, $P < 0.0001$, control vs TTX $P < 0.001$, control vs GYKI $P < 0.001$). These results suggest that the additional $CC1^+$ OL induced by either activity or AMPAR blockade exhibit a deficiency in the expression of at least one marker for mature myelin.

Effects of NMDAR blockade on OPC proliferation and differentiation

To determine whether NMDAR influence OPC development we examined OPC proliferation and differentiation in slice cultures treated with either the competitive NMDAR antagonist AP5 (Fig. 5Aiii), or the non-competitive inhibitor MK-801 (Fig. 5Aiv). For proliferation, one way ANOVA detected a significant source of variation between treatments groups ((ANOVA, F(2,707)= 3.26, $P < 0.05$). However, post-hoc analysis indicated that neither drug treatment was different to control (control vs AP5 $P > 0.05$, control vs MK-801 $P > 0.05$) (fig. 5B), with the source of variance arising from a modest reduction in the MK-801 group when compared to the AP5 treatment (AP5 vs MK-801 $P < 0.05$). The proportion of $BrdU^+$ $Olig2^+$ cells was similar between control and drug treated slices leading to the conclusion that NMDAR inhibition did not alter OPC proliferation in cerebellar slices.

For differentiation, treatment with AP5 produced a significant reduction in the proportion of $olig2^+$ cells expressing CC1 (ANOVA, F(2,548)= 12.36, $P < 0.0001$, control vs AP5 $P < 0.01$) (Fig. 6Biii, 6D), but this effect was not replicated in MK-801 treated

slices (Fig. 6Biv, 6D) (control vs MK-801 $P > 0.05$). AP5 was used at a concentration of 50 μM to match that used in other OPC studies (Li et al., 2013; Xiao et al., 2013; Lundgaard et al., 2013). Based on a standard logistic equation to describe drug interaction with receptors, 50 μM might be considered a supra-maximal concentration of AP5 as it exceeds the K_i for this compound by over an order of magnitude (e.g. AP5 Ki = 370 nM; Lodge et al., 1988), although the degree of antagonism afforded by AP5 in the preparation will be influenced by the concentration of glutamate at the receptor, which is unknown in the present preparation. However, since we considered that exposure of slices to this relatively high concentration of AP5 for 48 hours may have influenced OPC differentiation through non-NMDAR-mediated effects (i.e. 'off-target' interactions), the experiment was repeated with a lower concentration of AP5 (2.5 μM) that, while likely to still impact NMDAR, would reduce the likelihood of off-target effects. We also examined the effect of MK-801 at a reduced concentration (500 nM) since the initial concentration of 10 μM, while consistent with its use in the field, exceeded its Ki value considerably (30 nM, Wong et al., 1986). At these lower concentrations neither drug was found to affect differentiation (ANOVA, $F(2,511)= 1.042$, $P = 0.35$, control vs AP5 $P >0.05$, control vs MK-801 $P >0.05$) (Fig. 6Biii, 6D). The non-competitive nature of the antagonism by MK801 also simplifies interpretation with respect to the impact of unknown endogenous glutamate concentrations in the preparation. Hence, the lack of action of MK801 at either concentration, and the similar lack of effect of the lower concentration of AP5 on proliferation and differentiation, data do not support a role for NMDAR in the regulation of OPC development in cerebellar slice cultures.

NMDAR do not regulate OPC morphology

Potential functions of NMDAR in the morphological development of OPC were examined in slice cultures treated with AP5 (Fig. 7Ai-ii) and MK-801 (Fig. 7Bi-ii). OPC process extension, quantified by total branch length, and maximum Sholl intersection, were

unaffected by either AP5 (total branch length, t = 0.16, df = 45, *P* = 0.54; maximum Sholl intersection, t = 0.95, df = 45, *P* = 0.35) or MK-801(total branch length, t = 0.55, df = 86, *P* = 0.59; maximum Sholl intersection, t = 0.48, df = 86, *P* = 0.63) (Table 1). Similarly process branching was unaffected by either AP5 (total branch points, t = 0.84, df = 45, *P* = 0.40; total Sholl intersections, t = 0.45, df = 45, *P* = 0.66) or MK-801 (total branch points, t = 0.27, df = 86, *P* = 0.79; total Sholl intersections, t = 0.08, df = 86, *P* = 0.94) (Table 1). Further analysis of the Sholl data was performed to determine if blockade of NMDAR altered the spatial distribution of OPC process fields. The cumulative distribution of Sholl intersections, and the distance from the soma at which 50% of process intersections were registered, remained unchanged in OPC from either AP5 (Fig. 7Aiii, 7Aiv) (cumulative distribution, KS test, *D* = 0.18, *P* = 0.93; distance > 50% intersections, U = 256, *P* = 0.67) or MK-801 (Fig. 7Biii, 7Biv) (cumulative distribution, KS test, *D* = 0.24, *P* = 0.67; distance > 50% intersections, U = 817, *P* = 0.15) treated slice cultures. Overall, these data suggest that NMDAR do not influence the spatial distribution, or branching and extension of OPC processes in cerebellar slices.

DISCUSSION

This study develops our understanding of OPC development in three ways. First, it provides new findings on the influence of electrical activity and AMPAR on the morphological development of OPC. Second, it provides compelling evidence that AMPAR, but not NMDAR, contribute to the mechanisms connecting neuronal activity to these actions. Third, it presents new data indicating a role for AMPAR in promoting myelination *in situ*.

Influence of neuronal activity upon OPC proliferation and differentiation

TTX treatment increased OPC proliferation indicating that under basal conditions electrical activity within cerebellar axons restrains OPC proliferation. A similar impact

on OPC is observed *in vitro* where electrical stimulation of DRG-OPC co-cultures reduces OPC proliferation (Stevens et al., 2002), and *in vivo* where reductions in neuronal activity enhance it (Mangin et al. 2012). An anti-proliferative influence of neuronal activity is not a universal finding. Increased neuronal activity through physical exercise (Ehninger et al., 2011; Simon et al., 2011) and optogenetic stimulation (Gibson et al., 2014) increases OPC proliferation in the amygdala and cortex respectively, while activity blockade in the optic nerve decreases it (Barres and Raff, 1993). The influence of neuronal activity on OPC differentiation is also mixed. In the present work, TTX increased the number of OL expressing the mature marker CC1 showing that electrical activity within the slice normally inhibits OPC differentiation. However, as is the case with proliferation, other studies report a positive influence of action potentials that contrasts with the present findings (Gibson et al., 2014; Simon et al., 2011).

Multiple factors are likely to contribute to the diversity of responses exhibited by OPC to neuronal activity. Of particular relevance are anatomical location and developmental age, both of which vary greatly across the published literature, and which are known to influence a number of OPC parameters including proliferation (Hill et al., 2013), ion channel expression (Chittajallu et al., 2004; Fulton et al., 2010; Velez-Fort et al., 2010) and developmental fate (Rivers et al., 2008; Huang et al., 2014; Vigano et al., 2013). Developmental age may be of particular relevance since anti-proliferative effects of AMPAR activation are common to OPC originating from early postnatal tissue (Gallo et al., 1996; Yuan et al., 1998; and the present work), while positive influences on proliferation are shared by OPC in adult mice (Ehningher et al., 2011; Gibson et al., 2014; Simon et al., 2011). A focussed study analysing the correlation between anatomical location and developmental age is required to bring clarity to these issues.

Role of AMPAR in activity-dependent OPC development

OPC throughout the CNS express AMPAR that allow these cells to respond to glutamate released by neuronal activity (de Biase et al., 2010; reviewed by Gallo et al., 2008). Although these synaptic connections are lost during differentiation (De Biase et al., 2010) direct evidence connecting them to OPC development remains elusive. Previous work examined the influence of AMPAR agonists and antagonists on OPC isolated from cerebellar slice cultures (Yuan et al., 1998). In this study, OPC obtained from slices stimulated with AMPA showed decreased proliferation and differentiation, while blocking AMPAR increased these parameters. We used the non-competitive AMPAR antagonist GYKI to determine whether the AMPAR-dependent actions identified by Yuan et al. (1998) also hold for OPC retained and analysed within their native CNS environment. Treatment of cerebellar slices with GYKI for 48 hours produced an increase in both the proliferation of OPC and the number of OL expressing CC1. In agreement with the findings reported by Yuan et al., these data indicate that the activation of AMPAR inhibits the proliferation and differentiation of cerebellar OPC.

Whether these AMPAR-dependent actions involve synaptic connections between cerebellar axons and OPC remains to be determined. Certainly, the majority of OPC examined in this study were located in the molecular and granule cell layers where excitatory granule cell axons are located. Support for the synaptic regulation of OPC development can be found in other CNS tissue, for example the barrel cortex, where *in vivo* work confirms an inhibitory influence of AMPAR activation on OPC proliferation, and highlights a role for neuron-OPC synapses in these actions (Mangin et al., 2012). Here, bilateral whisker trimming, which reduced sensory input to the contralateral barrel cortex, resulted in a reduction of AMPA-mediated currents recorded from OPC. Importantly, this effect was restricted to OPC in the barrel cortex contralateral to the trimmed side, and was accompanied by an increase in the proliferation and density of OPC in this region. Overall, results obtained from cerebellar slices and the barrel cortex

provide compelling evidence that AMPAR activation on OPC provides a link connecting neuronal activity to the inhibition of OPC development. The specific modulation of AMPAR function in OPC is required to test this link directly.

Neuronal activity and AMPAR activation regulate the structure of OPC processes

Dynamic changes in process structure are fundamental to the development of OPC. They are required for OPC migration (Paez et al., 2009), and by definition must be integral to their ability to establish contact with target axons. While neuronal activity influences the branching and extension of mature OL (Makinodan et al., 2012) the impact of action potentials on OPC process morphology remains untested. Electrical activity appears to regulate cerebellar OPC development through the activation of AMPAR, and in agreement with this we found that blockade of both neuronal activity and AMPAR reduced the length and branching of OPC processes.

The induction of a mature morphology seems counter intuitive to the inhibitory effect that neuronal activity and AMPAR function exert on OPC development. How may these actions be reconciled? The simplest explanation is that different aspects of OPC maturation depend upon distinct mechanisms that are differentially regulated by neuronal activity (Lundgaard et al., 2013). For example, molecular differentiation, as indicated by a $CC1^+$ phenotype, may require activity-independent mechanisms, perhaps directed from cell-intrinsic developmental programmes (Zuchero and Barres, 2013), while morphological development may depend upon extrinsic activity-dependent signals mediated by AMPAR, and other ion channels and membrane receptors (Fulton et al., 2010; Stevens et al., 2002).

Blockade of neuronal activity or AMPAR activation increased differentiation leading to an expansion in the population of $CC1^+$ OL. What are the consequences of these actions

for myelination? Contrary to expectation, expansion in the population of $CC1^+$ OL was associated with a reduction in myelination indicating a failure in the ability of these cells to acquire a fully mature myelinating phenotype. In support of this, MBP expression, a key feature of OL maturation, was reduced by both TTX and GYKI. These treatments also altered the morphology of OPC by reducing process elongation and branching. An intriguing possibility is that cues critical for full differentiation are supplied through contact-mediated signalling mechanisms. Indeed, contact-dependent signalling involving neuregulin on axons and ErbB on OPC processes regulates OPC differentiation and myelination *in vivo* (Kim et al., 2003), and plays an important role in permitting activity-dependent myelination *in vitro* (Lundgaard et al., 2013). OPC with reduced morphological complexity, as occurs with TTX and GYKI treatments, would be expected to establish fewer axonal contacts and be deficient in contact-mediated signalling, while continuing to undergo cell-intrinsic developmental programmes. These intrinsic events may be sufficient to trigger molecular markers of maturation (e.g. $CC1^+$), but insufficient to promote the development of a full myelinating phenotype. Thus activity-dependent regulation of process development could guide OPC processes towards active axons where they may then obtain additional differentiation stimulating cues via contact-mediated signals. Whether neuronal activity stimulates process dynamics in OPC directly, and if contact-mediated cues then stimulate features of a mature myelinating phenotype remains to be seen.

Potential contribution of AMPAR to action potential driven OPC development

In this study, the effects of TTX and GYKI were compared in the same experiments providing an opportunity to test the involvement of AMPAR function in activity-dependent OPC development. TTX and GYKI act upon distinct targets (voltage gated Na^+ channels and AMPAR respectively) so their ability to induce common actions upon all of the OPC/OL parameters examined (proliferation, differentiation, process morphology,

myelination) suggest the hypotheses that OPC AMPAR provide a link connecting TTX sensitive activity-dependent signals to the regulation of OPC development, process extension and axon contact. However, it should be noted that in these experiments GYKI was added to the culture medium for 48 hours during which time it would also block neuronal AMPAR. Blockade of pre-synaptic excitatory neuronal input could produce indirect effects on OPC in two main ways. First, as indicated by our experiments with TTX, neuronal activity influences OPC development. Therefore, blockade of AMPAR by GYKI could have affected OPC indirectly through reductions in AMPAR-mediated excitatory network activity. Second, prolonged blockade of AMPAR may have lead to alterations in other neurotransmitter-mediated and activity-dependent signals, for example those involving GABAergic or purinergic signals (Stevens et al., 2002; Hamilton et al., 2008). Alterations in these signalling systems could then have influenced OPC independently of actions on OPC AMPAR. In spite of these limitations, the AMPAR-dependent actions on OPC development reported in this study, and their agreement with those obtained by the blockade of neuronal activity, provide the basis for new hypotheses, whose exploration will facilitate further progress on the question of OPC AMPAR functions. Exploring these ideas, and clarifying the role of OPC AMPAR in the effects we have reported, must await the development of more specific methods for targeting OPC AMPAR.

NMDAR do not regulate OPC development

Uncertainty persists as to whether NMDAR contribute to the development of OL and the generation of myelin since both appear normal in mice lacking the essential NR1 subunit (De Biase et al., 2011). Conversely, *in vitro* data from primary cultures suggest various functions for NMDAR including OPC migration and structural development (Li et al., 2013), myelin protein expression (Xiao et al., 2013) and myelination (Lundgaard et al., 2013). The acute manipulations of NMDAR function (pharmacological inhibitors,

shRNA) applied in these later studies may have revealed NMDAR-dependent functions masked by compensatory processes activated when NR1 is removed over extended periods *in vivo* (De Biase et al., 2011). Indeed, NR1 deletion was accompanied by an up-regulation in calcium permeable AMPAR that could potentially replace glutamate-mediated ion flux normally handled by NMDAR. Alternatively, the *in vitro* findings may represent artefacts arising from the use of OPC isolated from the influence of neuronal and glial cells present in the intact CNS.

To clarify inconsistencies between *in vitro* and *in vivo* studies, we performed *in situ* analyses of OPC in slice cultures treated with two structurally unrelated NMDAR antagonists that have distinct pharmacological modes of action. Slice cultures were ideal for this purpose since time-limited manipulations of receptor functions where possible within a preparation that largely preserved the arrangement of neural circuits and associated glial cells found in the CNS. The proliferation data indicated a modest reduction in the MK-801 group, but this was not supported by a key comparison with the control group, which revealed similar levels of proliferation. Proliferation in slices treated with AP5 were also comparable to those in the control group, thus overall, the data did not provide evidence to support an influence of NMDAR on OPC proliferation. Likewise, the morphological analysis of process outgrowth, branching, and field distributions indicated that neither drug affected these parameters.

While AP5 did not affect proliferation or process morphology, it was found to reduce the level of differentiation when comparisons were made to the control group. Interestingly, differentiation was not affected by a supra-maximal concentration of the non-competitive NMDA receptor antagonist, MK801. Since the levels of glutamate in the preparation will influence the degree of antagonism exerted by the competitive NMDA receptor, AP5, our initial interpretation was influenced to a greater extent by the null

effect of MK801. However, to explore this result further, the experiment was repeated with lower concentrations of both drugs. Critically, concentrations were selected that, while still likely to achieve at least a considerable blockade of the NMDAR, were more than an order of magnitude lower than the original concentrations used (AP5 2.5 μM, MK-801 500 nM). The reduction in differentiation detected when AP5 was applied at 50 μM was not observed at 2.5 μM. In contrast, the lower concentration of MK-801 replicated the null effect produced when this compound was applied at 10 μM. The lack of an impact of MK-801 at either concentration, taken together with the null effect observed at the lower concentration of AP5, suggest that NMDAR do not exert a positive influence on OPC differentiation in these slice cultures.

Unlike AMPAR, NMDAR channels exhibit a block at resting membrane potentials due to extracellular Mg^{2+} (Dingledine, 1999). Consequently, it could be argued that inhibitors of NMDAR would be expected to produce less dramatic effects on OPC development than those of AMPAR. In this context ineffectiveness of NMDAR blockers reported in this paper may be indicative of a low level of depolarisation in the slice cultures, rather than the lack of NMDAR function during OPC development. While this would certainly be true of neuronal NMDAR, the Mg^{2+} block of OPC and OL NMDAR is reported to be considerably weaker than that of neuronal NMDAR (3 to 5 fold block compared to 20-70 fold block for neuronal NMDAR, reviewed by Karadottir and Attwell, 2007). For this reason OPC NMDAR would be expected to mediate currents even at resting potentials. Consequently, any potential influence of NDMAR on OPC development, and the sensitivity of these processes to NMDAR blockade, might be expected to operate in relative freedom from the level of depolarisation. Overall, this argument, taken together with the present data on differentiation, proliferation and process morphology, support the conclusions drawn from earlier *in vivo* studies (De Biase et al 2011), namely that NMDAR are not a major requirement for OPC development.

This work introduces cerebellar slice cultures as a valuable model for studying activity-dependent oligodendrocyte development and myelination. Findings from this system indicate a differential involvement of AMPAR and NMDAR in OPC function, with an exclusive role for AMPAR in regulating molecular and morphological aspects of OPC development. Moreover, the identical actions of activity and AMPAR blockade indicate the potential for AMPAR signalling to form a functional link between neuronal activity and OPC development, and suggest that AMPAR in OPC provide a mechanism suitable for guiding the processes of these cells towards active target axons.

ACKNOWLEDGEMENTS

This work was supported by a Birmingham Science City Research Alliance Fellowship funded by the Higher Education Funding Council for England (HEFCE), and by an FP7 Marie Curie grant (CIG 294051). The authors thank Dr Markus Ehrengruber for SFV plasmids, Professor David Evans and Dr Eugene Ryabov for molecular biology reagents and advice, John Lapage for adapting the ITCN cell counter for batch image processing, Tessa Fulton-Lieuw for assistance with manual OPC reconstructions, Sandrine Wauters, Liliya Andrianova and Ghazala Begum for assistance with blinding experiments, Professor Bruno Frenguelli for use of the Zeiss HM 650V vibratome, Dr Andrew Powell for supplying MK-801, Professor Nicholas Barnes for helpful discussions on receptor pharmacology, and Dr Zubair Ahmed, Professor Martin Berry, and Dr Mark Wall for comments on the manuscript.

REFERENCES

Bakiri Y, Burzomato V, Frugier G, Hamilton NB, Karadottir R, Attwell D. 2009. Glutamatergic signaling in the brain's white matter. Neuroscience 158(1):266-74.

Barres BA, Raff MC. 1993. Proliferation of oligodendrocyte precursor cells depends on electrical activity in axons. Nature 361(6409):258-60.

Birgbauer E, Rao TS, Webb M. 2004. Lysolecithin induces demyelination in vitro in a cerebellar slice culture system. J Neurosci Res 78(2):157-66.

Chittajallu R, Aguirre A, Gallo V. 2004. NG2-positive cells in the mouse white and grey matter display distinct physiological properties. J Physiol 561(Pt 1):109-22.

De Biase LM, Kang SH, Baxi EG, Fukaya M, Pucak ML, Mishina M, Calabresi PA, Bergles DE. 2011. NMDA receptor signaling in oligodendrocyte progenitors is not required for oligodendrogenesis and myelination. J Neurosci 31(35):12650-62.

De Biase LM, Nishiyama A, Bergles DE. 2010. Excitability and synaptic communication within the oligodendrocyte lineage. J Neurosci 30(10):3600-11.

De Simoni A, Yu LMY. 2006. Preparation of organotypic hippocampal slice cultures: interface method. Nature protocols 1(3):1439-45.

Demerens C, Stankoff B, Logak M, Anglade P, Allinquant B, Couraud F, Zalc B, Lubetzki C. 1996. Induction of myelination in the central nervous system by electrical activity. Proc Natl Acad Sci U S A 93(18):9887-92.

Dingledine R, Borges K, Bowie D, Traynelis SF. 1999. The glutamate receptor ion channels. Pharmacol Rev 51(1): 7-61.

Ehninger D, Wang LP, Klempin F, Romer B, Kettenmann H, Kempermann G. 2011. Enriched environment and physical activity reduce microglia and influence the fate of NG2 cells in the amygdala of adult mice. Cell Tissue Res 345(1):69-86.

Ehrengruber MU, Renggli M, Raineteau O, Hennou S, Vaha-Koskela MJV, Hinkkanen AE, Lundstrom K. 2003. Semliki Forest virus A7(74) transduces hippocampal neurons and glial cells in a temperature-dependent dual manner. J neurovirol 9(1):16-28.

Ehrengruber MU, Schlesinger S, Lundstrom K. 2011. Alphaviruses: Semliki forest virus and Sindbis virus vectors for gene transfer into neurons. Current protocoL in neuroscience / editorial board, Jacqueline N Crawley [et al] Chapter 4:Unit 4.22.

Fulton D, Paez PM, Fisher R, Handley V, Colwell CS, Campagnoni AT. 2010. Regulation of L-type Ca++ currents and process mophology in white matter oligodendrocyte precursor cells by golli-myelin proteins. Glia 58:1292-1303.

Gallo V, Mangin JM, Kukley M, Dietrich D. 2008. Synapses on NG2-expressing progenitors in the brain: multiple functions? J Physiol 586(16):3767-81.

Gallo V, Zhou JM, McBain CJ, Wright P, Knutson PL, Armstrong RC. 1996. Oligodendrocyte progenitor cell proliferation and lineage progression are regulated by glutamate receptor-mediumted K^+ channel block. J Neurosci 16(8):2659-70.

Gibson EM, Purger D, Mount CW, Goldstein AK, Lin GL, Wood LS, Inema I, Miller SE, Bieri G, Zuchero JB and others. 2014. Neuronal activity promotes oligodendrogenesis and adaptive myelination in the mammalian brain. Science (New York, N Y) 344(6183):1252304.

Gudz TI, Komuro H, Macklin WB. 2006. Glutamate stimulates oligodendrocyte progenitor migration mediumted via an alphav integrin/myelin proteolipid protein complex. J Neurosci 26(9):2458-66.

Haber M, Vautrin S, Fry EJ, Murai KK. 2009. Subtype-specific oligodendrocyte dynamics in organotypic culture. Glia 57(9):1000-13.

Haber M, Zhou L, Murai KK. 2006. Cooperative astrocyte and dendritic spine dynamics at hippocampal excitatory synapses. J Neurosci 26(35):8881-91.

Hamilton N, Vayro S, Kirchhoff F, Verkhratsky A, Robbins J, Gorecki DC, Butt AM. 2008. Mechanisms of ATP- and glutamate-mediated calcium signaling in white matter astrocytes. Glia 56(7):734-49.

Hill RA, Patel KD, Medved J, Reiss AM, Nishiyama A. 2013. NG2 cells in white matter but not gray matter proliferate in response to PDGF. J Neurosci 33(36):14558-66.

Huang W, Zhao N, Bai X, Karram K, Trotter J, Goebbels S, Scheller A, Kirchhoff F. 2014. Novel NG2-CreERT2 knock-in mice demonstrate heterogeneous differentiation potential of NG2 glia during development. Glia 62(6):896-913.

Kim JY, Sun Q, Oglesbee M, Yoon SO. 2003. The role of ErbB2 signalling in the onset of terminal differentiation of oligodendrocytes in vivo. J Neurosci 23(13):5561-71.

Karadottir R, Attwell D. 2007. Neurotransmitter receptors in the life and death of oligodendrocytes. Neuroscience 145(4):1426-1438.

Li C, Xiao L, Liu X, Yang W, Shen W, Hu C, Yang G, He C. 2013. A functional role of NMDA receptor in regulating the differentiation of oligodendrocyte precursor cells and remyelination. Glia 61(5):732-49.

Lodge D, Davies SN, Jones MG, Millar J, Manallack DT, Ornstein PL, Verberne AJM, Young N, Beart PM. 1988. A comparison between the *in vivo* and *in vitro* activity of five potent and competitive NMDA antagonists. B J Pharmacol 95(3):957-965.

Lundgaard I, Luzhynskaya A, Stockley JH, Wang Z, Evans KA, Swire M, Volbracht K, Gautier HOB, Franklin RJM, Charles F-C and others. 2013. Neuregulin and BDNF induce a switch to NMDA receptor-dependent myelination by oligodendrocytes. PLoS biology 11(12):e1001743.

Makinodan M, Rosen KM, Ito S, Corfas G. 2012. A critical period for social experience-dependent oligodendrocyte maturation and myelination. Science (New York, N Y) 337(6100):1357-60.

Mangin J-M, Li P, Scafidi J, Gallo V. 2012. Experience-dependent regulation of NG2 progenitors in the developing barrel cortex. Nature neuroscience 15(9):1192-4.

Ouardouz M, Durand J. 1991. GYKI 52466 antagonizes glutamate responses but not NMDA and kainate responses in rat abducens motoneurones. Neuroscience letters 125(1):5-8.

Paez PM, Fulton DJ, Spreuer V, Handley V, Campagnoni C, Macklin WB, Colwell CS, Campagnoni AT. 2009. Golli myelin basic proteins regulate oligodendroglial progenitor cell migration through voltage-operated Ca^{++} influx. J Neurosci 20:6663-76.

Paternain AV, Morales M, Lerma J. 1995. Selective antagonism of AMPA receptors unmasks kainate receptor-mediumted responses in hippocampal neurons. Neuron 14(1):185-9.

Patneau DK, Wright PW, Winters C, Mayer ML, Gallo V. 1994. Glial cells of the oligodendrocyte lineage express both kainate- and AMPA-preferring subtypes of glutamate receptor. Neuron 12(2):357-71.

Rishal I, Golani O, Rajman M, Costa B, Ben-Yaakov K, Schoenmann Z, Yaron A, Basri R, Fainzilber M, Galun M. 2013. WIS-NeuroMath enables versatile high throughput analyses of neuronal processes. Developmental neurobiology 73(3):247-56.

Rivers LE, Young KM, Rizzi M, Jamen F, Psachoulia K, Wade A, Kessaris N, Richardson WD. 2008. PDGFRA/NG2 glia generate myelinating oligodendrocytes and piriform projection neurons in adult mice. Nat Neurosci 11(12):1392-401.

Salter MG, Fern R. 2005. NMDA receptors are expressed in developing oligodendrocyte processes and mediumte injury. Nature 438(7071):1167-71.

Schneider CA, Rasband WS, Eliceiri KW. 2012. NIH Image to ImageJ: 25 years of image analysis. Nature methods 9(7):671-5.

Simon C, Gotz M, Dimou L. 2011. Progenitors in the adult cerebral cortex: cell cycle properties and regulation by physiological stimuli and injury. Glia 59(6):869-81.

Stevens B, Porta S, Haak LL, Gallo V, Fields RD. 2002. Adenosine: a neuron-glial transmitter promoting myelination in the CNS in response to action potentials. Neuron 36(5):855-68.

Velez-Fort M, Maldonado PP, Butt AM, Audinat E, Angulo MC. 2010. Postnatal switch from synaptic to extrasynaptic transmission between interneurons and NG2 cells. J Neurosci 30(20):6921-9.

Vigano F, Mobius W, Gotz M, Dimou L. 2013. Transplantation reveals regional differences in oligodendrocyte differentiation in the adult brain. Nature neuroscience 16(10):1370-2.

Wake H, Lee PR, Fields RD. 2011. control of local protein synthesis and initial events in myelination by action potentials. Science (New York, N Y) 333(6049):1647-51.

Wearne SL, Rodriguez A, Ehlenberger DB, Rocher AB, Henderson SC, Hof PR. 2005. New techniques for imaging, digitization and analysis of three-dimensional neural morphology on multiple scales. Neuroscience 136(3):661-80.

Wong EH, Kemp JA, Priestley T, Knight AR, Woodruff GN, Iversen LL. 1986. The anticonvulsant MK-801 is a potent N-methyl-D-aspartate antagonist. Proc Natl Acad Sci U S A 83(18):7104-8.

Xiao L, Hu C, Yang W, Guo D, Li C, Shen W, Liu X, Aijun H, Dan W, He C. 2013. NMDA receptor couples Rac1-GEF Tiam1 to direct oligodendrocyte precursor cell migration. Glia 61(12):2078-99.

Yuan X, Eisen AM, McBain CJ, Gallo V. 1998. A role for glutamate and its receptors in the regulation of oligodendrocyte development in cerebellar tissue slices. Development 125(15):2901-14.

Zuchero JB, Barres BA. 2013. Intrinsic and extrinsic control of oligodendrocyte development. Current opinion in neurobiology 23(6):914-20.

FIGURE LEGENDS

Figure 1. Blockade of neuronal activity and AMPAR increases OPC proliferation. **A.** General experimental design. For the majority of experiments, slice cultures were incubated for 6 days in control medium before addition of drugs. Drugs or control medium were replaced 24 hours later with the inclusion of BrdU in experiments studying proliferation. Slices were also infected with SFV on this day in experiments examining OPC morphology. Slice cultures were fixed at 8 DIV. **B, C, D.** MIP images illustrating immunoflourescent labeling of olig2 and BrdU, and colocalisation results for control **(B)**, TTX **(C)** and GYKI **(D)** treated slice cultures. Left panels: Typical olig2 (red) (**Bi, Ci, Di**) and BrdU (green) (**Bii, Cii, Dii**) signals. Right panels (**Biii, Ciii, Diii**): threshold colocalisation images obtained from fields shown in left panels. White pixels indicate areas of colocalisation. Arrows indicate olig2$^+$ BrdU$^+$ cells. Scale = 20 μm. **E.** The average % olig2$^+$ cells displaying BrdU label was significantly higher in OPC exposed to either TTX or GYKI (control 22.1 % ± 1.3, TTX 27.5 % ± 1.3, GYKI 27.5 % ± 1.7). * significance at $P < 0.05$. Data are expressed as means ± SE.

Figure 2. Blockade of neuronal activity and AMPAR increases differentiation. **A - C.** MIP images illustrating immunoflourescent labeling of olig2 and CC1, and colocalisation results for control **(A)**, TTX **(B)** and GYKI **(C)** treated slice cultures. Left panels: Typical olig2 (green) (**Ai, Bi, Ci**) and CC1 (red) (**Aii, Bii, Cii**) signals. Right panels (**Aiii, Biii, Ciii**): threshold colocalisation images obtained from fields shown in left panels. White pixels indicate areas of colocalisation. Arrows indicate olig2$^+$ CC1$^+$ cells. Scale = 20 μm. **D.** The average % olig2$^+$ cells expressing CC1 protein was significantly greater in OPC treated with either TTX or GYKI (control 51.2 % ± 1.3, TTX 72.7 % ± 1.1, GYKI 63.6 % ± 1.2). *** significance at $P < 0.001$. Data are expressed as means ± SE.

Figure 3. Blockade of neuronal activity and AMPAR reduces OPC process extension and branching. **A.** NG2 protein expression confirms OPC identity of GFPf labeled cells. **Ai**. Typical putative GFPf labelled OPC with a small irregular shaped cell body and a complex array of fine processes. **Aii**. Immunolabelling for NG2 from the same field displayed in Ai. **Aiii**. Merge of images in Ai-ii confirming overlap of GFPf and NG2 signals. **B-D.** MIP GFPf images (left panels, i), 3D volume renderings (middle panels, ii), and Neuronstudio reconstructions (right panels, iii) taken from control (B), TTX (C) or GYKI (D) treated slice cultures. Scale bars in A-D = 20 μm. **E**. Average process length was significantly reduced in OPC exposed to either TTX or GYKI (control 1435.3 μm ± 244.4, TTX 782.9 μm ± 64.3, GYKI 802.9 μm ± 88.6). **F**. The average number of OPC process branch points was significantly reduced after exposure to either TTX or GYKI (control 59.9 ± 3.6, TTX 46.0 ± 4.7, GYKI 44.7 ± 3.5). * significance at $P < 0.05$. Data are expressed as means ± SE.

Figure 4. Blockade of either neuronal activity or AMPAR suppresses myelination. **A**. In situ immunohistochemical assay for myelination. Fluorescent MIP images with typical NF200 (**Ai**) and MBP (**Aii**) signals in a control slice. **Aiii**. Thresholded merge image reveals areas of NF200/MBP colocalisation (white pixels). Yellow arrows indicate potential myelin internodes. **B-C**. Reduced myelination in slice cultures treated with either TTX (**B**) or GYKI (**C**). MIP images display typical NF200 (**Bi, Ci)** and MBP (**Bii, Cii**) signals from TTX and GYKI treated slice cultures. **Biii, Ciii**. Areas of NF200/MBP colocalisation (white pixels) from TTX and GYKI fields seen in Bi-ii and Ci-ii respectively. **D.** Myelination indexed by the ratio of colocalised pixels / NF200 pixels. Both TTX and GYKI produce a significant decrease in colocalisation (control 0.39 ± 0.01 %, TTX 0.29 ± 0.02 %, GYKI 0.27 ± 0.01 %). **E**. Average threshold MBP pixels expressed as ratio of the total image pixel count. Treatment with either TTX or GYKI reduced MBP signals

(control 0.25 ± 0.007 %, TTX 0.21 ± 0.019 %, GYKI 0.17 ± 0.005 %) Scale bars = 50 μm. *** significance at $P < 0.001$ Data are expressed as means ± SE.

Figure 5. Blockade of NMDAR does not alter OPC proliferation.

A. Immunofluorescence assay for proliferation. **Ai**. Merged MIP image showing a representative pattern of olig2 (red) and BrdU (green) signals in a control-treated slice culture. **Aii**. Colocalisation image for the control field shown in Ai. White pixels indicate areas of colocalisation, arrows indicate example olig2$^+$/BrdU$^+$ cells. **Aiii-iv**. Typical colocalisation images for AP5 (Aiii) and MK-801 (Aiv) treated slice cultures. Scale = 20 μm. **B**. The average percentage of BrdU$^+$ Olig2$^+$ cells is not altered by either AP5 or MK-801 (control 43.2 % ± 0.01, AP5 44.8 % ± 0.01, MK-801 41.8 % ± 0.01).

Figure 6. Impact of NMDAR blockade on OPC differentiation. **A**. Immunofluorescence assay for differentiation in slice cultures treated with AP5 (50 μM) and MK-801 (10 μM). **Ai**. Merged MIP image showing a representative pattern of olig2 (green) and CC1 (red) signals in a control-treated slice culture. **Aii**. Colocalisation image for the control field shown in Ai. White pixels indicate areas of colocalisation. **Aiii-iv**. Typical colocalisation images for AP5 (Aiii) and MK-801 (Aiv) treated slice cultures. **B**. Examination of differentiation in slice cultures treated with AP5 (2.5 μM) and MK-801 (500 nM). **Bi**. Merged MIP showing olig2 (green) and CC1 (red) labeling in a control slice. **Bii**. Colocalisation image for the field shown in Bi. **Biii**-**Biv**. Colocalisation images for AP5 (Biii) and MK-801 (Biv) treated slice cultures. Arrows indicate example olig2$^+$/CC1$^+$ cells. Scale = 20 μm. **D**. Treatment with 50 μM AP5, but not 10 μM MK-801, reduced the percentage of CC1$^+$ olig2$^+$ cells in slice cultures (control 42.3 % ± 0.01, AP5 37.7 % ± 0.01, MK-801 45.3 % ± 0.01). **E**. The average percentage of CC1$^+$ Olig2$^+$ cells is not altered by either 2.5 μM AP5 or 500 nm MK-801 (control 32.07 % ± 0.009, AP5 34.02 % ± 0.009, MK-801 32.94 % ± 0.008). ** significance at $P < 0.01$ Data are expressed as

means ± SE.

Figure 7. Activation of NMDAR does not regulate the spatial distribution of OPC process fields. **A**. Spatial distribution of process fields in OPC treated with AP5. **Ai-ii**. NeuroMath reconstructions of representative OPC from control (Ai) and AP5 (Aii) treated slice cultures. Sholl analysis was performed with concentric circles at 5 μm intervals from a starting radius 20 μm from the centre of the soma. For clarity only circles at intervals of 20 μm are shown (dashed circles). **Aiii**. Cumulative probability distribution for Sholl intersections. Intersections made by the processes of AP5 treated OPC display a similar spatial profile to those of control OPC. **Aiv**. The average distance from the soma at which 50% of intersections occur is unchanged by treatment with AP5. **B**. Spatial distribution of process fields in OPC treated with MK-801. **Bi-ii.** Reconstructions of OPC from control (Bi) and MK-801 **(**Bii) treated slice cultures. Sholl analysis and representative concentric circles as described above for Ai-ii. **Biii**. Analysis of the cumulative distribution of sholl intersections indicates a similar spatial profile for control and MK-801 treated OPC. **Biv**. The average distance from the soma at which 50% of intersections are registered is not altered by treatment with MK-801. Scale bars = 20 μm. Data are expressed as means ± SE.

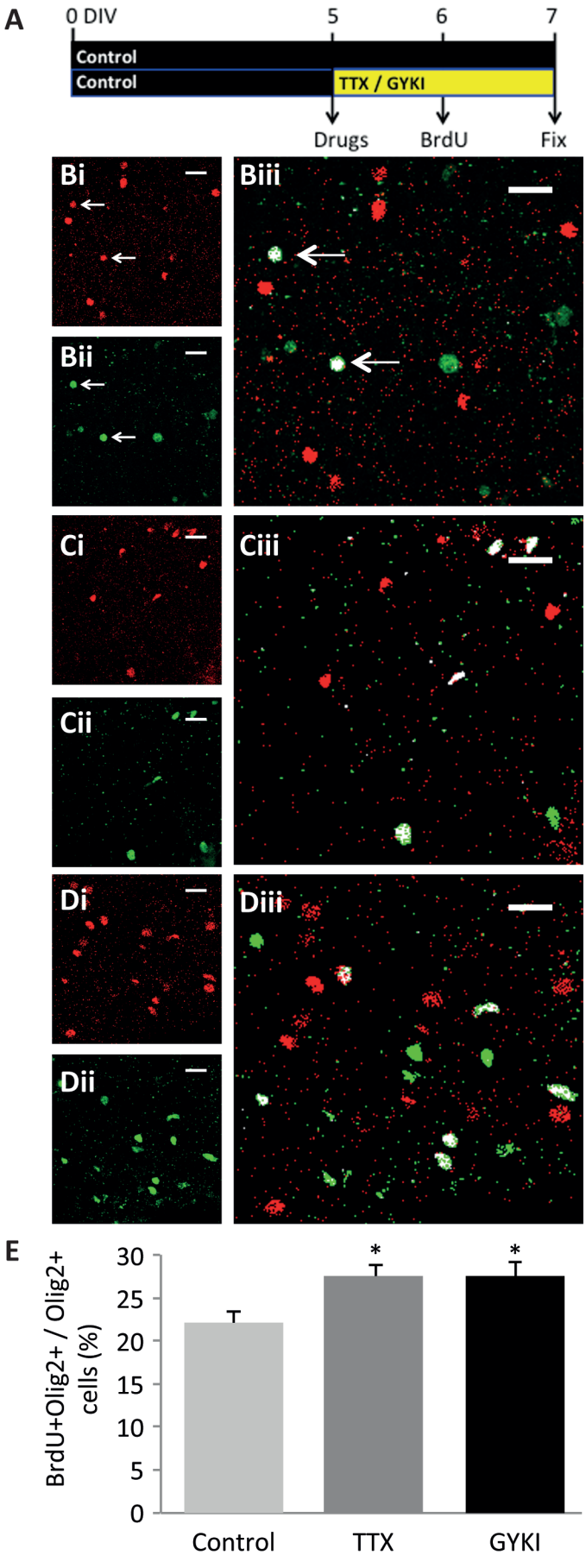
A
0 DIV
5
6
7
Control
Control
TTX / GYKI
Drugs
BrdU
Fix
Bi
Bii
Biii
Ci
Cii
Ciii
Di
Dii
Diii
E
BrdU+Olig2+ / Olig2+ cells (%)
30
25
20
15
10
5
0
*
*
Control
TTX
GYKI

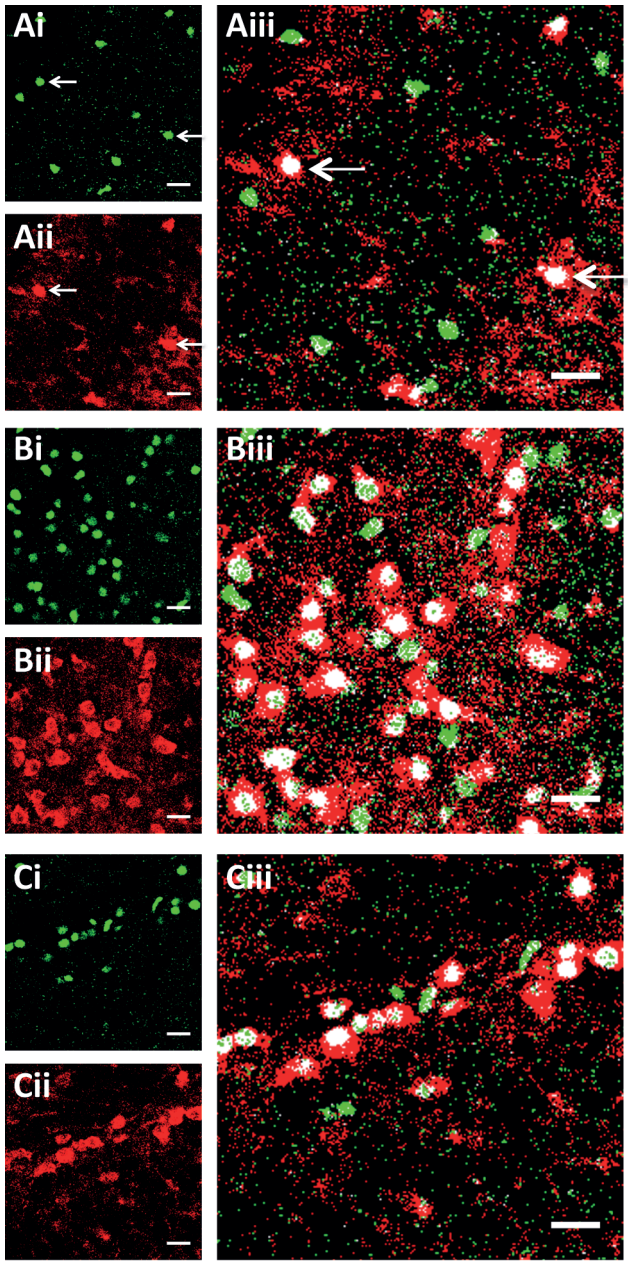
Ai
Aii
Aiii
Bi
Bii
Biii
Ci
Cii
Ciii

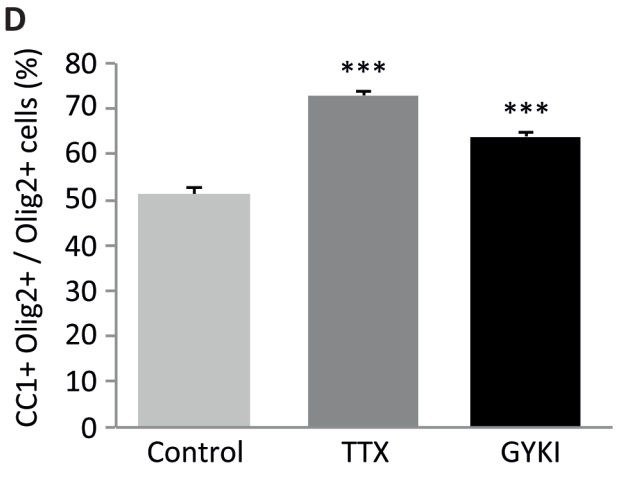
D
CC1+ Olig2+ / Olig2+ cells (%)
80
70
60
50
40
30
20
10
0
***
***
Control
TTX
GYKI

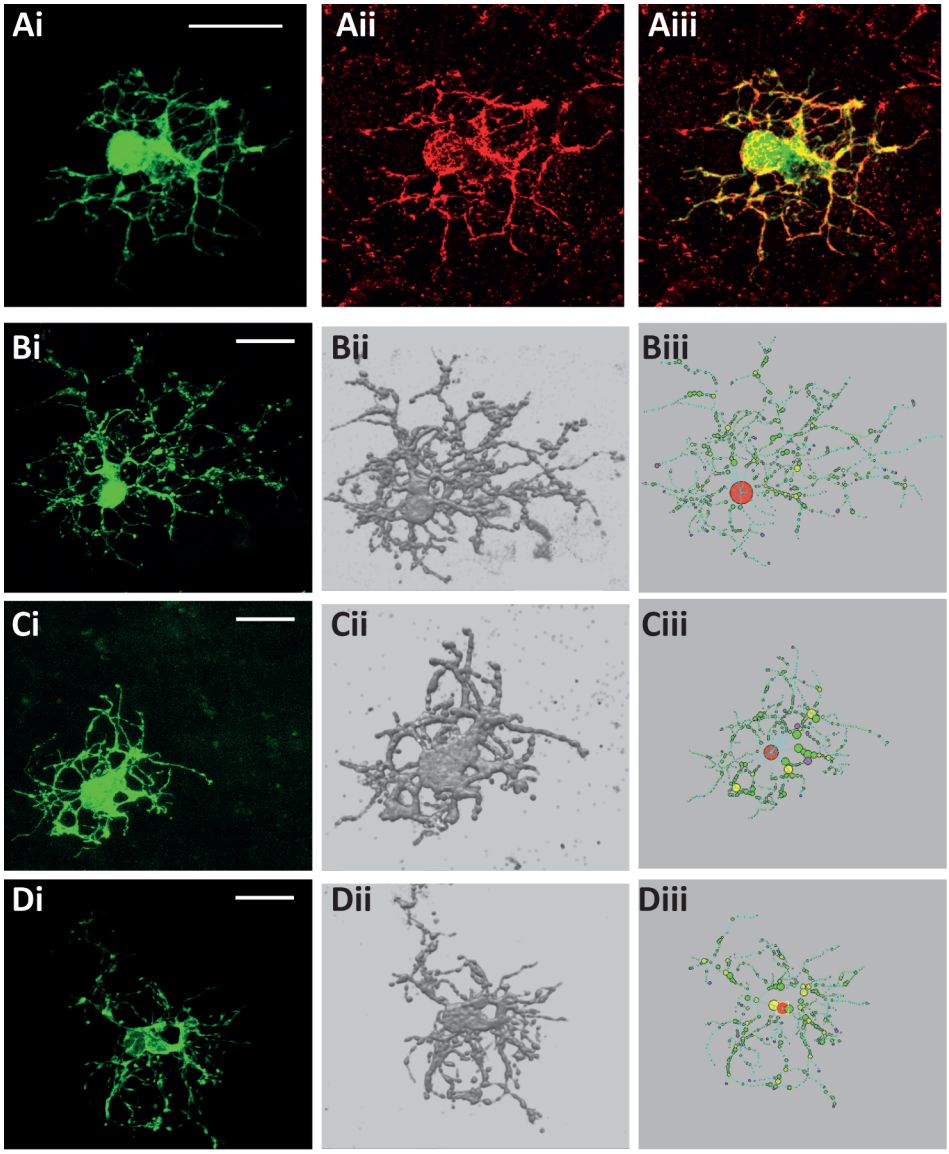
Ai
Aii
Aiii
Bi
Bii
Biii
Ci
Cii
Ciii
Di
Dii
Diii

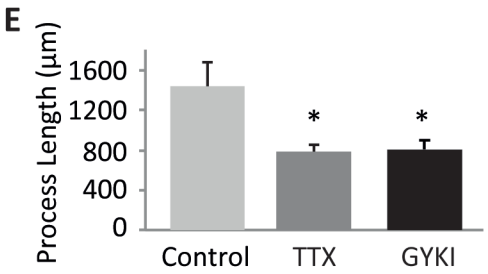
E
Process Length (µm)
1600
1200
800
400
0
*
*
Control
TTX
GYKI

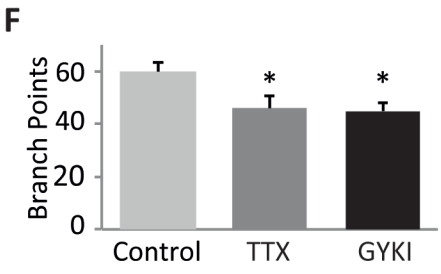
F
Branch Points
60
40
20
0
*
*
Control
TTX
GYKI

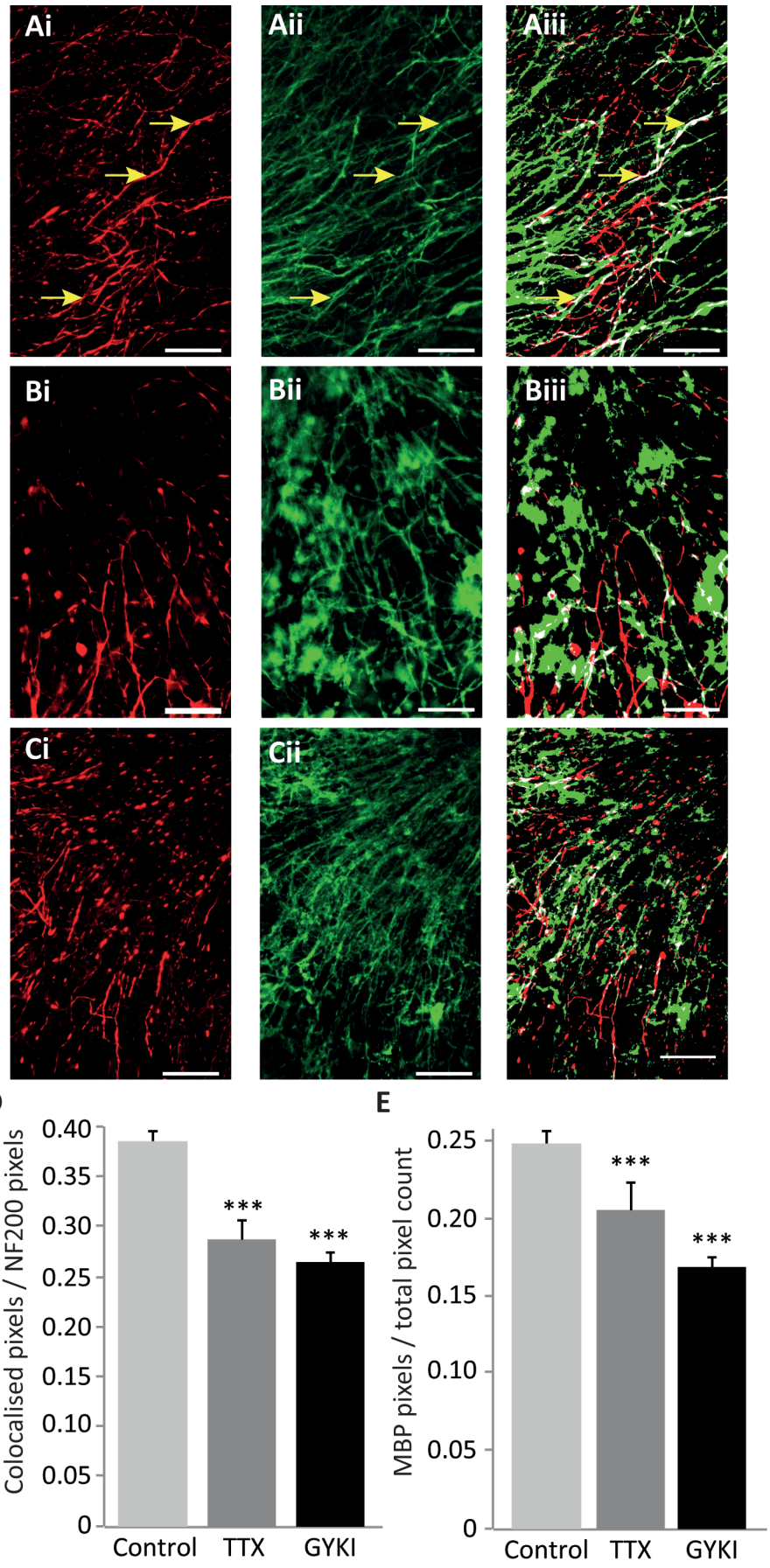
Ai
Aii
Aiii
Bi
Bii
Biii
Ci
Cii
D
Colocalised pixels / NF200 pixels
0.40
0.35
0.30
0.25
0.20
0.15
0.10
0.05
0
***
***
Control
TTX
GYKI
E
MBP pixels / total pixel count
0.25
0.20
0.15
0.10
0.05
0
***
***
Control
TTX
GYKI

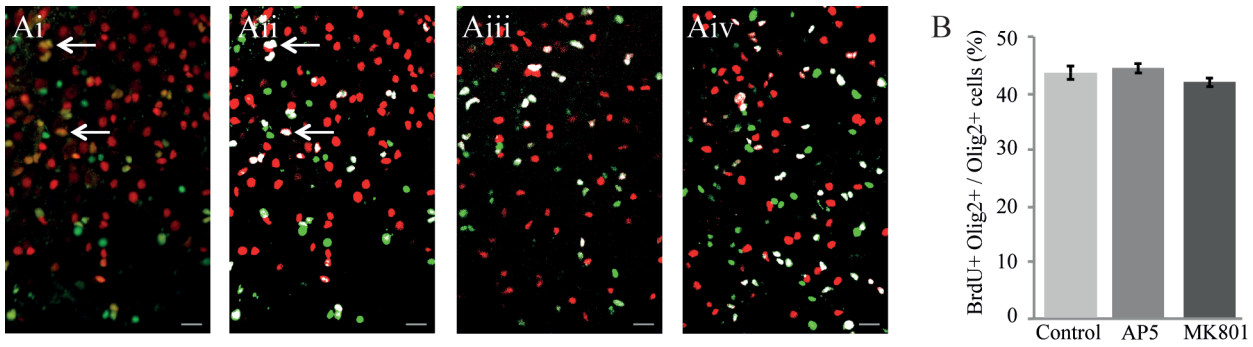
Ai
Aii
Aiii
Aiv
B
BrdU+ Olig2+ / Olig2+ cells (%)
50
40
30
20
10
0
Control
AP5
MK801

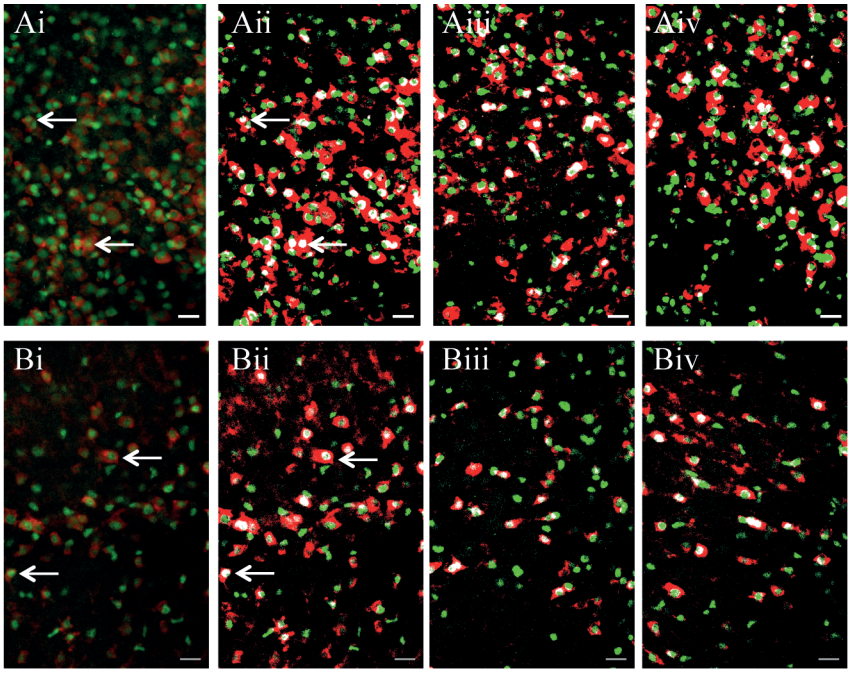
Ai
Aii
Aiii
Aiv
Bi
Bii
Biii
Biv

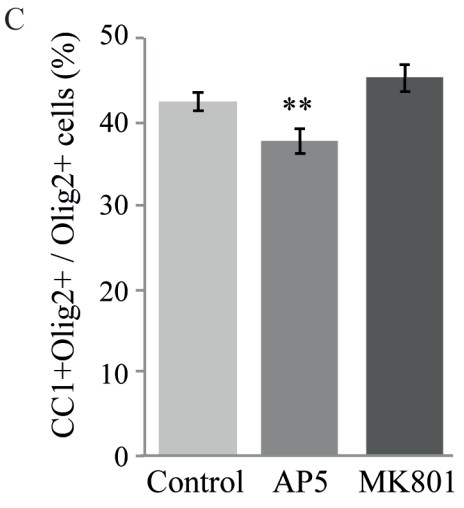
C
CC1+Olig2+ / Olig2+ cells (%)
50
40
30
20
10
0
**
Control
AP5
MK801

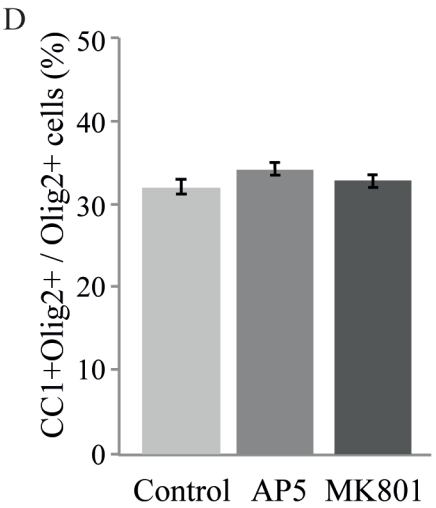
D
CC1+Olig2+ / Olig2+ cells (%)
50
40
30
20
10
0
Control
AP5
MK801

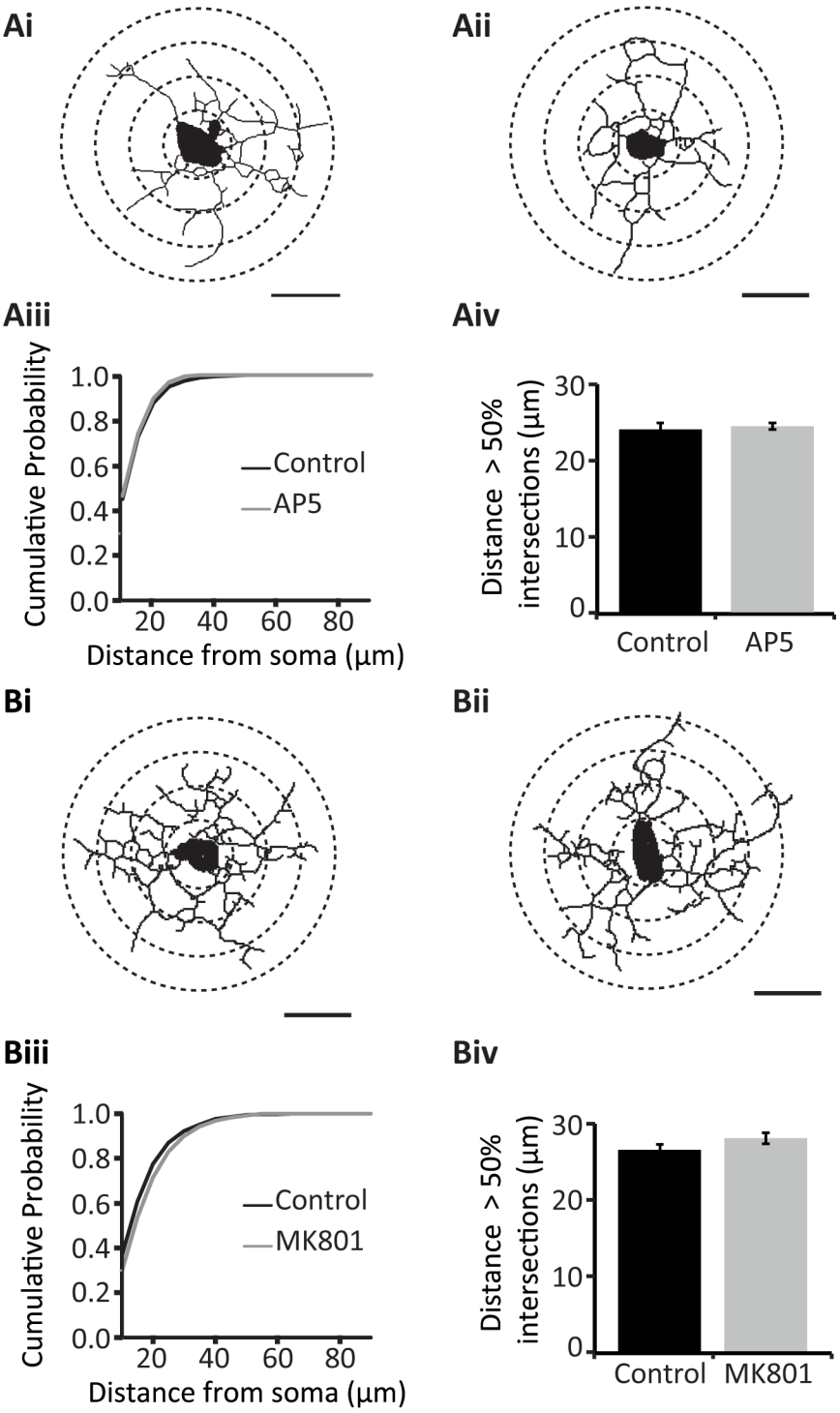
Ai
Aii
Aiii
Aiv
Cumulative Probability
1.0
0.8
0.6
0.4
0.2
0.0
20
40
60
80
Distance from soma (µm)
Control
AP5
Distance > 50% intersections (µm)
30
20
10
0
Control
AP5
Bi
Bii
Biii
Biv
Cumulative Probability
1.0
0.8
0.6
0.4
0.2
0.0
20
40
60
80
Distance from soma (µm)
Control
MK801
Distance > 50% intersections (µm)
30
20
10
0
Control
MK801

Table 1. Branch lengths and branch points in OPC treated with AP5 and MK801

	AP5		MK801	
	Control	Drug	Control	Drug
Total Branch Length (μm)	410 ± 31	439 ± 36	539 ± 37	511 ± 32
Max Sholl Intersection (μm)	38 ± 2.1	35 ± 1.1	46 ± 2.2	47 ± 1.7
Total Branch Points	96 ± 12.8	83 ± 8.9	82 ± 6.8	80 ± 5.9
Total Sholl Intersections	29 ± 3.8	26 ± 3.5	45 ± 4.4	46 ± 3.4

SUPPLEMENTARY RESULTS

Fannon et al.

Neuronal activity and AMPA-type glutamate receptor activation regulates the morphological development of oligodendrocyte precursor cells

Validation of NeuroMath automated tracing method

We validated the automated tracing method by comparing it directly with data analysed by the NeuronStudio manual tracing method. For this work, a subset of OPC (control n= 12, MK801 n = 11), originally traced automatically for the MK801 study (Fig. 7), were re-traced manually and the resulting reconstructions quantified for total process length and number of branch points (Fig. S1). Absolute values for process length and branch points differed between the automated and manual tracing methods. For example, total outgrowth measured from control OPC was greater when determined by the manual tracing method (Fig. S1C) (manual tracing 648 ± 52 μm, automated tracing 471 ± 35 μm). In contrast, automated tracing produced estimates of total branch point number that were greater than those resulting from manual tracing (Fig. S1D) (e.g. for control OPC, manual tracing 42.1 ± 5.3, automated tracing 76.8 ± 9.7). Importantly, these between-methods differences were consistent across treatments (Fig. S1C,D), and experiments (Fig. S2 C,D), such that NeuroMath estimates for total process outgrowth were always lower than those produced by NeuronStudio, while estimates of branching were always greater. NeuronStudio (manual method) estimates of process outgrowth are likely to be greater as the underlying models are 3D and so include process projections in the Z axis, which is not the case in the 2D models generated by NeuroMath (automated method). Similarly, the 2D nature of the NeuroMath reconstructions likely underlies the greater level of branching detected by this software, since process

crossings that are separated in the Z axis may be miss-interpreted as branch points when the Z dimension is compressed to a single plane.

Despite these differences in the estimation of process length and branching, both methods reliably detected the same between treatment results. Specifically, both the automated and manual tracing methods showed that that neither process length, nor branching differed between the control and MK801 treated OPC (Fig. S1C, Fig S1D). These observations were confirmed by two-way ANOVA which revealed significant differences in process length due to tracing method (automated vs manual) [$F(1,45) = 12.65$, $P < 0.001$], but not from treatment (control vs MK801) [$F(1,45) = 1.21$, $P = 0.28$]. Critically, there was no interaction between tracing method and treatment [$F(1,45) = 0.07$, $P = 0.78$] indicating that the performance of the two methods was comparable. The same outcomes were found when the frequency of branch points was analysed, with a two way ANOVA, indicating significant effects from tracing method [$F(1,45) = 23.24$, $P < 0.0001$], but not from treatment [$F(1,45) = 0.44$, $P = 0.51$]. Again, there was no interaction between tracing method and treatment [$F(1,45) = 0.1$, $P = 1.00$], providing further confirmation that the two methods reliably detected the same between-treatment trends.

Further validation of the automated tracing method was sought by re-analysing data originally traced using the manual method. Here we selected a data set that was originally shown to contain significant differences between the treatments, thus providing an opportunity to re-affirm a positive result. For this work control and TTX treated OPC (Fig. 3) were re-traced in NeuroMath (Fig. S2), quantified for total process length and total branch points (Fig. S2C, D). As seen in the previous comparison (Fig. S1C), absolute values for process length differed between the two methods (e.g. control OPC total outgrowth NeuronStudio 1435 ± 244 μm, NeuroMath 995 ± 57 μm). However,

both methods detected the same significant reduction in the TTX group (t = 2.396, df = 52 , $P < 0.05$). (cf. Fig. S2C and Fig. 3E). Similarly, while absolute values for total branch points differed between the two programs, when comparisons were made between the control and TTX treatments, NeuroMath returned a similar result to NeuronStudio, namely a reduction in the number of branch points that approached significance (t = 1.838, df = 52, $P = 0.07$) (cf. Fig. S2D and Fig. 3F).

Overall, the comparisons described above indicate that the automatic tracing method provides a reliable means to make between treatment comparisons. The present study uses comparisons between control and drug treatments to determine effects on process development. Relative differences of this kind operate independently of absolute values, therefore, the use of two different tracing approaches is justified so long as conclusions are only drawn from results obtained using the same tracing method.

Supplementary Figure 1. Manual re-tracing of OPC analysed by automated methods produced equivalent results. **A-B**. Comparison of reconstructions obtained using manual and automated tracing methods from control (A) and MK801 (B) treated OPC. **Ai, Bi.** Representative MIP of $GFPf^{+}$ OPC used for manual and automated cell tracing. **Middle panels:** 3D volume renderings **(Aii, Bii)** and the underlying models **(Aiii, Biii)** generated through NeuronStudio. **Aiv, Biv**. Reconstructions of the OPC shown in previous panels prepared using NeuroMath automated tracing method. Scale bars = 20 μm. **C, D.** Quantification of process outgrowth (C) and branching (D) indicate that NeuronStudio and NeuroMath detect similar between-group results for Control and MK801 treated OPC. *** indicate significance at $P < 0.001$ for between methods comparisons. Data are expressed as means ± SE.

Supplementary Figure 2. Automated re-tracing with NeuroMath replicates the

between-treatment results obtained by manual tracing. **A-B.** Comparison of reconstructions obtained from GFPf labelled control (A) and TTX (B) treated OPC. Representative GFPf MIP images (**Ai**, **Bi**) and their reconstructions prepared in NeuronStudio (**Aii**, **Bii**) and NeuroMath (**Aiii**, **Biii**) for control (A) and TTX (B) treated OPC. Scale bars = 20 μm. **C-D**. Quantification of OPC process fields from NeuroMath tracings. The average total outgrowth (C) of OPC processes is significantly reduced in OPC from TTX-treated slice cultures. Near-significant reduction in the number of branch points in OPC from TTX-treated slice cultures. * significance at $P < 0.05$. Data are expressed as means ± SE.

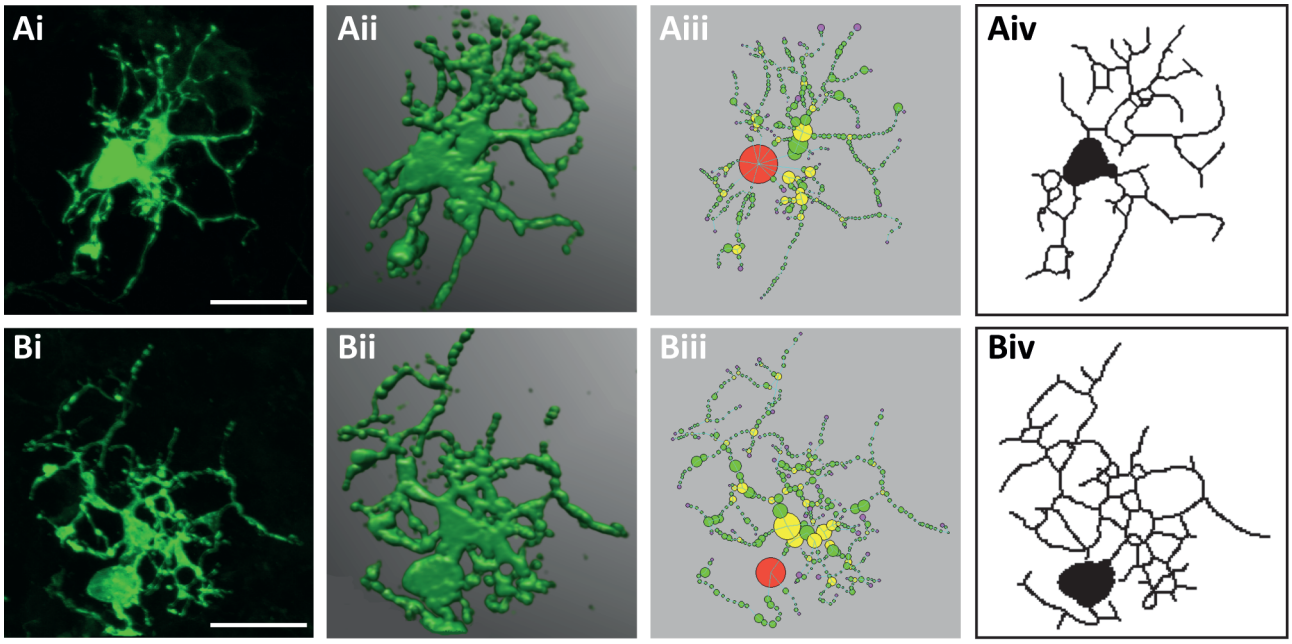
Ai
Aii
Aiii
Aiv
Bi
Bii
Biii
Biv

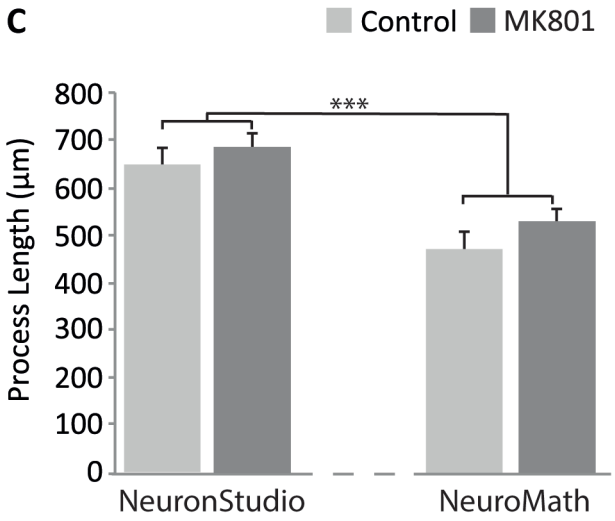
C
Control
MK801
Process Length (µm)
800
700
600
500
400
300
200
100
0
***
NeuronStudio
NeuroMath

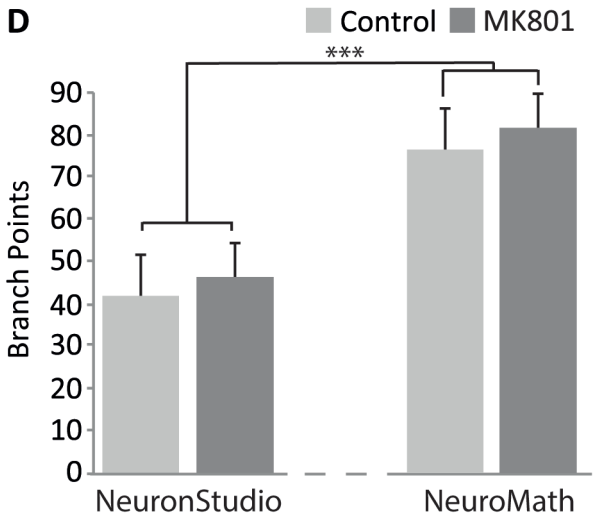
D
Control
MK801
Branch Points
90
80
70
60
50
40
30
20
10
0
***
NeuronStudio
NeuroMath

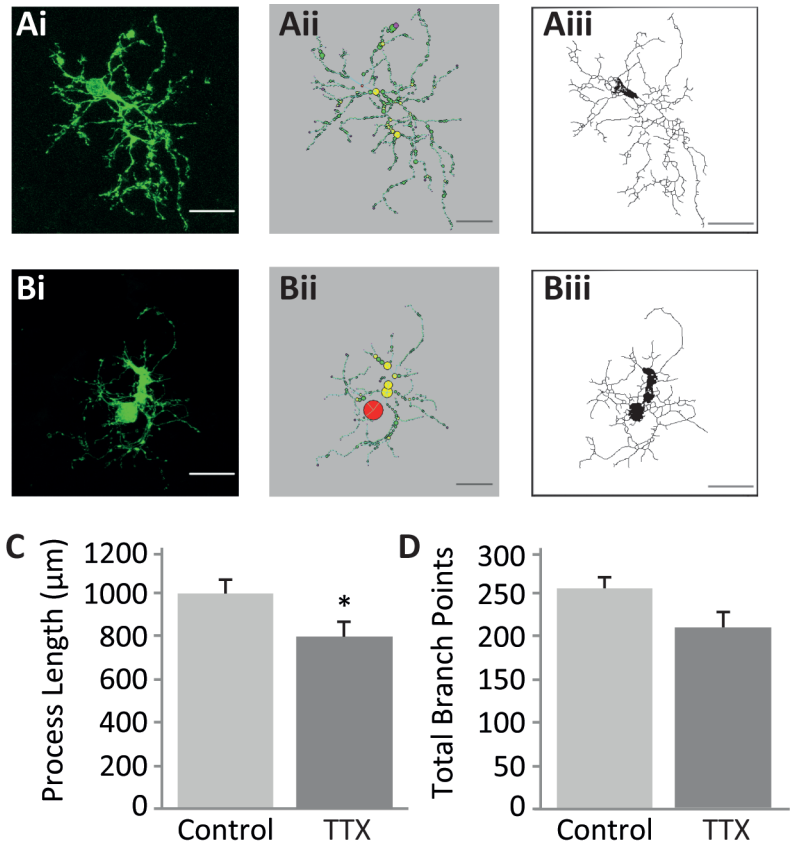
Ai
Aii
Aiii
Bi
Bii
Biii
C
Process Length (µm)
1200
1000
800
600
400
200
0
*
Control
TTX
D
Total Branch Points
300
250
200
150
100
50
0
Control
TTX